Residual Strain in a Reservoir Ice Cover

Huang, Wenfeng

2018-08

Huang , W , Li , Z , Leppäranta , M , Han , H & Wang , N 2018 , ' Residual Strain in a Reservoir Ice Cover : Field Investigations, Causes, and Its Role in Estimating Ice Stress ' Journal of Hydraulic Engineering (New York) , vol. 144 , no. 8 , 04018048 . https://doi.org/10.1061/(ASCE)HY.1943-7

http://hdl.handle.net/10138/246371
https://doi.org/10.1061/(ASCE)HY.1943-7900.0001488

The Residual Strain in a Reservoir Ice Cover: Field Investigations, Causes, and Its Role in Estimating Ice Stress

Wenfeng Huang[1], Zhijun Li[2], Matti Leppäranta[3], Hongwei Han[4], Ni Wang[5]

[1] Lecturer, Key Laboratory of Subsurface Hydrology and Ecological Effects in Arid Region of the Ministry of Education, School of Environmental Science and Engineering, Chang'an University, Xi'an 710054, China (Corresponding author). E-mail: huangwenfeng@chd.edu.cn

[2] Professor, State Key Laboratory of Coastal and Offshore Engineering, Dalian University of Technology, Dalian 116024, China. E-mail: lizhijun@dlut.edu.cn

[3] Professor, Department of Physics, University of Helsinki, Helsinki 00014, Finland. E-mail: matti.lepparanta@helsinki.fi

[4] Lecturer, School of Water Conservancy and Civil Engineering, Northeast Agricultural University, Harbin 150030, China. E-mail: hhw777@sina.com

[5] Lecturer, Key Laboratory of Subsurface Hydrology and Ecological Effects in Arid Region of the Ministry of Education, School of Environmental Science and Engineering, Chang'an University, Xi'an 710054, China (Corresponding author). E-mail: 282864934@qq.com

Abstract: Ice strain dominates the ice thrust and dynamics on reservoir dams and retaining structures. An exclusively designed laser range finder was deployed to measure the surface ice displacements along six directions at a reservoir in northeastern China. The incompletely confined boundary (ice-boundary bonding), ice cracks development, water level fluctuation, parallel crack dynamics, allow the surface ice to move rather than keep still in response to thermal deformation/pressure, and thus cause the ice strain deviates from thermal strain. Consequently, a residual strain was introduced and calculated from the recorded displacements. Observations showed that the residual strains were anisotropic and showed diurnal patterns following the air/ice temperature. A scale dependence of crack development was observed and causes potential scale effects to residual strains. The real ice strain consists of thermal strain and residual strain. The proportion of the latter increased as time went by. A modified constitutive law accommodating the residual strains was developed to evaluate the impacts of the residual strains and to estimate the surface ice stresses. Modeling results underlined the role of the residual strain in determining both the principal stress and the stress perpendicular to the dam face. The residual strain is probably the reason why the observed ice stress is always much lower than the single thermal stress.

Keywords: thermal strain; residual strain; constitutive law; static ice loads; reservoir ice

Introduction

Although dams have been built and operated for a long time in northern climate, the forces exerted by ice on them are still not well understood. These loads must be taken into consideration in design of ice-infested hydraulic structures and engineering (Cox 1984; Bouaanani et al. 2004), but there is still not enough information available to predict these loads with a satisfactory confidence for engineers (Comfort et al. 2000a,b; Gebre et al. 2013). Horizontal ice forces on structures are usually divided into two broad categories: static forces produced by a structure restraining the thermal expansion of an ice cover in horizontal plane, and dynamic forces created by the interaction of moving ice cover with a fixed/moving structure.

Ice pressure is an important stress value to be measured in determining the static loads of ice (Comfort et al. 2003; Taras et al. 2009). Previous findings have revealed that the ice pressure in

reservoirs can arise from various processes that can act alone or in combination. Among these processes, one can identify thermal forces (Cox 1984; Xu 1994; Comfort et al. 2003), forces associated with changes in water level (Stander 2006; Taras et al. 2009) and wind forces (Prinsenberg et al. 1997). Furthermore, in situ data and theoretical analyses also indicate that the magnitude of thermal ice load is affected by the snow/slush cover, ice thickness, shoreline confinement, reservoir shape, and relative stiffness of various hydraulic structures (Boulton and Jones 1979; Comfort et al. 2000b,c; Arunachalam 2005; Petrich et al. 2015). Most of the theoretical predictions of the maximum ice thrust are based on a simple-plane compressive model of fragmented ice floes with respect to buckling/bending and hinging effects (Carter et al. 1998), which derives an upper bound for ice thrust. Instead, some empirical functions have been reported to show encouraging ability to estimate the thermal loads of an ice cover based on the elastic and viscous behavior of ice (Xu 1986; Bergdahl 1978; Cox 1984; Fransson 1988). Current models consistently overestimate the ice stress, but the reasons for this overestimation are still not well understood (Azarnejad and Hrudey 1998; Comfort et al 2003).

Conventionally, field measurements of ice thrust/load rely on various stress sensors frozen between ice and dam face, or within ice. However, occasional detachments and poor bonds between ice and sensors contaminate the data quality. Therefore, ice deformation or strain measurement provides an indirect way to determine the ice stress in a reservoir (Morse et al. 2009, 2011). Additionally, the ice push and sudden displacement due to the release of cumulated ice stress/strain can damage the dam revetments, installed hydrostructures, and even buildings on the shore (Comfort and Liddiard 2006). Hence, the determination of the ice strains and their accumulation is of great importance in understanding and modeling the ice thrust in lakes and reservoirs. Nevertheless, ice displacement and strain have not been well quantified especially in field scale.

A field campaign was conducted between February 24 and March 26 in 2011 to monitor the surface ice displacement in Hongqipao Reservoir, northeastern China. This paper presents the in situ investigations and results, aiming at quantifying the residual strain within the ice cover and relating it to environmental conditions to better understand the mechanism of ice thrust. A new constitutive model was then developed to estimate the ice stress and to evaluate the effects of

environmental conditions besides the air/ice temperature.

Field Investigations

Hongqipao Reservoir (46°N, 125°E) is located in Daqing, Heilongjiang Province, northeastern China. The reservoir area is 35 km^2 with a storage capacity of 1.1×10^8 m^3, bound at the western, southern and eastern sides by concrete-paved earth-filled dams. The dams are totally 24.5 km long. Ice season usually begins in later October or early November when the air temperature descends below 0°C and ends in middle or late April. Ice thickness can be up to 1.20 m in March when the air temperature is still below the freezing point of freshwater (Fig. 1). Over the whole ice season, water replenishing is ceased, although one intake works for water supply. The water level fell by only 0.05 m from 147.18 m to 147.13 m during the two weeks of measurement, and the current velocity under ice was assumed to be negligible (Fig. 2).

An automatic laser range finder (LRF) was developed exclusively to measure the distance (i.e. displacements of surface ice) along any direction. LRF consists mainly of parts: a high-resolution laser range finder (Leica Disto D3A) and a steerable automatically-rotating base. The ranger finder has an accuracy of ±1 mm (with a reading resolution of 0.1 mm) within the measuring range of 0.05~200 m. The rotating base has a direction accuracy of ±1°. These two parts were modulated and connected to a laptop, which functioned as a controller and data logger. The field design and instrumentation is shown in Fig. 3. Six reflectors (Points P1 ~ P6) were fixed and refrozen quickly into the ice cover around the LRF (Point O) to reflect the laser transmitted by the LRF for distance recording. All reflectors were spaced 60° apart from one another, with P1 pointing to the geographic north. The lengths of the lines OP1, OP2, ..., OP6 were 4.9 m, 7.9 m, 10.8 m, 13.9 m, 16.9 m and 19.9 m, respectively. The LRF was at about 40 m distance from the dam face.

In order to avoid the contamination in the displacement data induced by wind force and surface melting of snow/ice, the LRF was fastened to a platform through 4 screws. The platform had three 90 cm-long wooden legs (like a tripod), all of which were inserted into the ice sheet to a depth of approximately 50~60 cm (similar to the technology deployed in polar ice observations by Polashenski et al. (2012)). The platform was carefully leveled using a bubble level before its legs

were refrozen fasten into the ice holes. Every reflector had also a 90 cm long wooden leg, which was inserted into the ice cover to a similar depth (50~60 cm). Therefore, the maximum heights of the LRF and reflectors were lower than 40 cm beyond the ice surface, reducing the wind effect. Furthermore, all surfaces and legs of the reflectors and LRF platform were colored white to avoid radiative absorption that might induce internal melting at the ice-void interfaces.

A meteorological station was established 30 m away from the LRF to measure and record the net radiation, air temperature, and wind speed and direction once a minute. A thermistor chain was placed into a drill hole, and refrozen into the ice cover to measure the ice/water temperature at 2-122 cm below the ice surface and 25 cm vertical spacing (at 2 cm, 7 cm, 12 cm, 17 cm, 22 cm, 27 cm, 32 cm, 42 cm, 52 cm, 62 cm, 82 cm, 92 cm, 102 cm, and 122 cm). The resolution was 0.1 ¡C for temperature, 1 W/m^2 for irradiance, 0.1 m/s for wind speed, and 1° for wind direction. An ultrasound sonar with ~2 cm accuracy was placed 50 cm below the ice bottom to record the ice thickness at every half hour. The initial ice thickness was 90 cm when the ice was instrumented on February 24. Meanwhile, ice thickness was also measured manually every two or three days using an ice auger. All measurements were ended on March 28 when the piles tilted.

However, due to power and machinery failure, surface ice displacement datasets were obtained discontinuously before March 4. And the data recorded after March 20 was false since the reflector stands started to become loose due to ice melt. Therefore, a 16-day period of good data was obtained and is further analyzed here.

Constitutive Laws

Current Constitutive Laws

In order to illustrate thermal ice displacements directly, we assume that the ice cover (or the surface layer) is isothermal and homogeneous all time, and that the ice temperature changes instantaneously. Fig. 4 illustrates the thermally induced ice deformation under three kinds of constraint boundaries (free, fixed, and incompletely confined ends) when the ice temperature changes. The points O and P_i denote the LRF and an arbitrary reflector in Fig. 3.

Under the free boundary condition, with an increment in ice temperature, ΔT_i (°C), the length of

129 OP, expands from its initial L_0 to L_T,

130 $$L_T = L_0(1+\varepsilon_T), \quad (1)$$

131 where α is the thermal expansion coefficient of freshwater ice ($\sim 5.0 \times 10^{-5}$ °C^{-1}). There is no stress
132 within the ice cover.

133 Under the fixed boundary (i.e. completely confined), points O and P never move with changes
134 in temperature for an intact ice cover, and the thermal strain ε_T and stress σ_T (Pa) can be expressed
135 as

136 $$\varepsilon_T = \frac{L_T - L_0}{L_0} = \alpha \Delta T, \quad (2)$$

137 $$\varepsilon_T = E_i^{-1} \sigma_T = E_i \Delta T, \quad (3)$$

138 where E_i (Pa) denotes the elastic modulus assuming the ice is an elastic medium. Usually,
139 freshwater ice is regarded as an [illegible] medium and modeled using a Maxwell unit (a
140 spring, which represents instantaneous elastic deformation, in series with a nonlinear dashpot
141 based on a power law creep which models the nonrecoverable viscous deformation) (Bergdahl
142 1978; Azarnejad and Hrudey 1998; Petrich et al. 2015). Thermal ice pressure can be formulated as

143 $$\frac{d\varepsilon_i}{dt} = E_i \left(\frac{d\sigma_i}{dt} + KD \left(\frac{\sigma_i}{\sigma_0} \right)^n \right), \quad (4)$$

144 where t is time (s), D is the temperature-dependent viscous creep rate (s^{-1}), K (m^{-2}) and n are
145 viscous rheology parameters, σ_0 is a reference stress (Pa), and the subscript i stands for the ice.
146 The first and second term in the square brackets represent the instantaneous elastic strain and
147 time-dependent viscous strain, respectively.

148 Taking into consideration the material nature of freshwater ice, some complicated
149 physically-based models primarily consisting of a Maxwell unit in series with a Kelvin-Voigt unit
150 (i.e. a spring parallel to a nonlinear dashpot, representing the delayed elastic deformation) or other
151 combinations of several Maxwell and/or Kelvin-Voigt units have been proposed (Yamaoka et al.
152 1988; Ivchenko 1990). However, comparisons with analytical results and field tests indicated that
153 the models including only a Maxwell unit (Eq. (4)) show a better prediction and require less
154 computing consumption (Azarnejad and Hrudey 2001; Petrich et al. 2015).

The ice strain rate is currently considered to be equal to the thermal strain rate (Bergdahl 1978; Cox 1984; Timco et al. 1996; Petrich et al. 2015)

$$\frac{d\varepsilon_i}{dt} = \frac{d\varepsilon_T}{dt} = \alpha \frac{dT}{dt}. \quad (5)$$

Thus, Eq. (4) is transformed into

$$\frac{d\varepsilon_i}{dt} = E_i \left(\alpha \frac{dT}{dt} * KD + \frac{\sigma_i}{\eta_0} \right). \quad (6)$$

A New Constitutive Law

Under incompletely confined boundary (e.g. elastic restraint), which is representative of natural static lake and reservoir ice covers, especially for a tilted dam, the ice cover also expands (thick black dotted lines in Fig. 4) but not as much as the free boundary, i.e., the length grows to L_B with an increase in ice temperature. Therefore, the real ice strain

$$\varepsilon_i = \varepsilon_T + \varepsilon_R = \alpha \Delta T + \frac{L_B - L_0}{L_0}, \quad (7)$$

where L_0 and L_B are the original distance and the distance after a temperature change, respectively, and the residual strain

$$\varepsilon_R = \frac{L_B - L_0}{L_0} \quad (8)$$

was determined from the displacements of the LRF and reflectors.

Eq. (6) is thus transformed into

$$\frac{d\varepsilon_i}{dt} = E_i \left(\frac{d}{dt}(\alpha T * \varepsilon_R) * KD + \frac{\sigma_i}{\eta_0} \right). \quad (9)$$

This represents a modified Maxwell constitutive model with linear elastic and nonlinear viscous parts. The residual strain would cause the ice stress to deviate from those created by the thermal strain alone.

What Is the Residual Strain ε_R?

The residual strain ε_R is defined as Eq. (8), and is introduced to the most common constitutive law (Eq. (6)), representing the responses of the surroundings to changes in ice temperature (i.e.

thermal stresses), for instance, the ice edge dynamics on the tilt dam face and land slopes and along the parallel cracks, the development of surface cracks, and the water level fluctuations.

If it is assumed that the intact ice cover (without cracks and ridges) is fixed completely to the reservoir boundaries (dams and land slopes), reflectors in Fig. 3 and 4 should not move in response to a temperature change, and the ice strain consists solely of thermal strain (Eq. (2)). Actually, physical processes in response to the thermal loads drive the piles to move back and forth, thus producing the residual strain. For instance, the ice edges indeed move forwards and backwards restrainedly (adhesive sliding) on the dam faces or slopes due to the thermal expansion and contraction of ice cover (Fig. 5), somehow releasing the thermal stress (Morse et al. 2009, 2011). Tensile stresses due to ice contraction or shear stresses give rise to intensive cracks and fissures especially within the surface layer of the ice cover (Fig. 5a). With a rise in ice temperature (Fig. 5b), old cracks close, and the target pile moves from P(a) to P(b) due to thermal expansion. With (Fig. 5c), the ice cover contracts, the closed cracks open, and new cracks occur for the ice cannot hold high tension because of its low tensile strength. Therefore, the target pile P(b) usually does not return to its original place (a), P but to P(c), causing an accumulated displacement. The opening and closing of the cracks also absorb thermal strains. The reservoir shape can cause a spatial variability of thermal strains. Moreover, the ice cover bending and buckling due to the rise/fall of water stage inevitably creates additional surface strains (Stander 2006). The time series of the distance between P were observed and recorded by the LVDT. We are currently not able to partition the contributions of all above processes, but they are embodied jointly in the residual strain. In other words, the ice strain should consist of thermal strain and residual strain (Eq. (7)).

Data Processing

Dry and wetted cracks develop extensively over the reservoir ice cover and have a significant impact on the static ice strain/stress and loads (Azarnejad and Hrudey 1998), especially the prolonged parallel and circumferential cracks breaking the ice cover (Carter 1998; Comfort et al. 2003). In order to investigate the general features of surface cracks, 138 individual snapshots of ice cracks and an image mosaic covering a ~550 m area (Jia 2012) were reanalyzed using

image processing method similar to Huang et al. (2016) to explore the crack density (crack area per unit ice surface area) and its spatial variation. Within differing spatial scales from 2 m to 24 m, the averaged crack densities and their standard deviation (STD) were calculated.

$$\rho_{R14} = \frac{\sum L_1 + \sum L_4}{L_1 + L_4} \Big/ \frac{\sum L_4}{L_4}$$

$$\rho_{R25} = \frac{\sum L_2 + \sum L_5}{L_2 + L_5} \Big(\Big/ \frac{\sum L_5}{L_5} \Big)$$

$$/_{R36} = \frac{" L_3 + " L_6}{L_3 + L_6}$$

Field Code Changed

In order to calculate the static stress (load) of surface ice using Eq. (9), a thin surface layer is assumed to be detached from the ice cover for modeling purpose (similar to Bergdahl (1978), Morse et al. (2009), and Petrich et al. (2015)). The averaged value of air and 2 cm depth temperature is assumed to be the representative temperature of the thin surface layer.

Results and Analysis

Ice Thickness and Temperature

When the field campaign was established, there was a discontinuous snow cover due to uneven accumulation by winds. The thickness of snow 2 m around Point O was up to 30 cm, while only about 3 cm thick or less snow was distributed at other points. No new snow fell through the entire instrumented period. Snow cover melted away on March 15 when air temperature rose above 0 °C. Much melt water accumulated in depressions of ice surface.

The ice cover grew or melted quite slowly, and in the period of the experiment the ice thickness remained within 93 ± 2 cm.

The ice temperature above 35 cm depth followed the variations of daily air temperature cycle with damping and lag increasing with depth (Fig. 7). Although the diurnal variations in ice temperature below 35 cm depth were negligible, there was a gradual increase due to rising mean air temperature, enhancing solar radiation, and cold/warm spells. The ice temperature at 2 cm depth was much closer to air temperature during the last few days due to surface melting and ablation.

After a few stable diurnal cycles with daily mean value of −9 °C in phase (a), the representative

ice temperature increased with diurnal oscillations to a peak (-1.0 °C) in phase (b), decreased to -10.0 °C in phase (c), and then rose sharply to approximately 0 °C within two days (phase (d)). Through the observation, northern winds prevailed, and the mean wind speed (2 m above the ice surface) was 3.5 m/s.

The Observed Residual Strain

The observed residual strain was generally lower than thermal strain for an arbitrary temperature increment (Fig. 8). Since their initial positions, surface ice mostly contracted along the directions of P1, P2, and P4, and expanded along P3, P5, . Although the ice cover was constrained by the firm boundaries, along all directions (P1 ~ P6), the ice showed a diurnal cycle of expansion and contraction in response to the daily evolution of air/surface ice temperature, and also a seasonal variability following the cold/warm spells.

But there are generally differences between expansions and contractions within the same day (Fig. 8), leading to growing accumulated permanent displacements. In addition, within an individual phase of temperature rise/fall, the ice displacement was able to shift from expansion to contraction, or conversely, such as P1, P2, and P4 in phase (c).

Obviously, the P1 displacement differed significantly in magnitude and pattern from others. And the P2 displacement gave little physical senses since it roughly contracted but P6 (in the same line) expanded. The scale variability of the spatial distribution of surface cracks is likely . For a static ice cover, flaws and cracks exist densely over the ice surface due to compressive, tensile, and shear stresses caused by water level variations, winds, as well as temperature changes. Crack image processing (Fig. 9) indicated that the averaged crack densities beyond 2 m scale are coincidently 4.6%~4.9% and show little scale dependence, but their STD values show a significant scale dependence, namely, STD decrease from 2.2% to 0.9% as the spatial scale increases from 2m to 12m, and remain around 0.9% when the scale grows beyond 12 m. Therefore, the displacement can be impacted the spatial variability of crack development if the length between reflectors and LRF is less than 12 m (such as P1, P2, and P3).

On the other hand,

Consequently, the displacement datasets from

are favorably representative of the entire ice cover, and were used to calculate the ice strain/stress.

Surface Ice Strain

Eq. (7) gives the surface ice strain taking into consideration the observed residual strain. Figure 10 presents the strains perpendicular and parallel with the nearby dam and the first principal strain with its direction derived from lines P4, P5, and P6. All directional and principal strains showed significant discrepancies from the thermal strains, especially after the warm spell (phase (b)), though they show similar temporal trends.

As the residual strains accumulated with time, the discrepancies between the directional (also normal and parallel) strains also increased gradually, perhaps due to the piling up and climbing of ice onto the dam face, crack formation and evolution, and ice creep (Fig. 5).

Estimate of Surface Ice Stress

Taking into consideration the observed residual strains, a modified constitutive model was developed to estimate the ice stresses (Eq. (9)). The values of all involved parameters and coefficients are assigned in Table 1. The principal stresses showed similar trends with the ice temperatures and thermal stresses (Fig. 11), but the principal stresses were quite close to the thermal stresses except during the temperature surge (phase (d)). The normal stresses were always lower than the thermal ones, especially they were lower by more than 250 kPa (~35%) during the warm spells, indicating the residual strains created a considerable relief to the thermal loads normal to the dam face. This argued that a significant error can be produced by the ignorance of environmental responses to thermal loads, for instance, ignorance of ice dynamics on the dam face, the development and evolution of cracks, the changes in water level (Stander 2006; Taras et al. 2009), and wind stresses (Prinsenberg et al. 1997).

Strain Rates

Conventionally, the maximum ice load is believed to occur when the ice cover fails on the dam face in compression. The compressive strength of freshwater ice determines the maximum load. Freshwater ice is a viscoelastic medium with a strain rate dependent compressive strength. For strain rate lower than 10^{-4}/s, ice shows ductile behavior, and its strength increases in way of a power law function against an increased strain rate. For the strain rate larger than 10^{-3}/s, ice is brittle, and its strength decreases rapidly with increasing strain rate. Within the ductile-brittle transition zone (10^{-4} ~ 10^{-3}/s), the peak strength is reached, approximately 3 MPa at 0 °C (Zhang et al. 2012). The time derivatives of Eq. (2), (8) and (7) provide the strain rates of thermal strain, residual strain, and surface ice strain, respectively (Fig. 12). The strain rates of the thermal strain and residual strain are of similar magnitude (10^{-9} ~ 10^{-7}/s), which is consistent with the field observations by Morse et al (2009). But the integrated strain rate has a wider range (10^{-11} ~ 10^{-6}/s magnitude). At this range, the compressive strength is lower than ~1.4 MPa (-1°C), and the elastic modulus is believed to be lower than 1.5 GPa (Han et al. 2016). This is also the reason why the stress borne by the dam face should not surpass 1.4 MPa (e.g. Fig. 11, Morse et al. 2009; Taras et al. 2009) and why the elastic modulus used in Table 1 is much lower than the values (~9 GPa) usually used before.

Discussion

The Capability of LRF and Uncertainties

The surface ice displacements were measured in a plain reservoir of northeastern China using a laser ranging device. This study gave an opportunity to directly quantify the deviations of real ice strain to thermal strain. The deployed LRF provided excellent, site-, real-time measurements of surface ice displacements. Relatively, conventional contact strain and stress sensors can cause significant systematic errors when the expansion coefficient of the sensor material is close to that of ice, while LRF is free of this problem. LRF can measure the motion of adequate length to cover the universal impacts of field-scale crack development (e.g. scale >12 m in the studied reservoir), which is almost impossible to be reproduced in cold laboratories. However, the ability

of the present device is also limited by some uncertainties. According to the present measurements, the LRF with an accuracy of 1 mm is not able to effectively detect the diurnal changes in displacement, namely, its accuracy predetermines a minimum effective measuring distance, of which the deformation can be effectively sensed. For instance, the minimum distance should be larger than in Hongqipao Reservoir.

Another uncertainty in LRF measurements is induced by the wind-induced vibration of reflectors. Although we were intended to reduce the exposure heights of LRF and reflectors, the wind-induced distortions (often at high frequency) bring some fluctuations to the displacement datasets. These fluctuations are more significant in P2-P3 than P4-P6, but don't contaminate their diurnal and seasonal dynamic regimes. These fluctuations and measuring errors can be removed using filtering process, for instance, centered moving average was used in this study.

The LRF and reflectors movement induced by surface and internal ice melt are able to significantly contaminate the displacement data. Appropriate technical procedures should be applied to rule out this melt effects, e.g. hole refreezing method used in this study and Polashenski et al. (2012). Nevertheless, careful inspection is further required to check the displacement series and to remove sudden or abnormally rapid changes.

Comparisons with Other Results

The recorded surface displacements of ice cover are direct evidences suggesting that the real ice strain is not equal to the thermal strain alone though thermal strain plays a dominant role. The surface displacements were detected not only at far sites (e.g. the present results) but also significantly at near-field sites (i.e. near dam face), even for vertical dam faces (Morse et al. 2009). All processes governing these displacements need to be investigated to simulate the static ice loads accurately. The observed residual strains increased gradually with obvious daily variability.

consistent with other investigations (e.g. Morse et al. 2009, 2011).

The proposed constitutive model underlines the role of ε_R in evaluating the static ice loads toward the dam face. The calculated stresses perpendicular to the dam were up to 600 kPa, favorably consistent with the near-dam stresses but much greater than the far-field stresses measured by Morse et al (2009) and Taras et al (2009). Comparisons indicated that the near-field movement is often greater than the far-field by 2~3 orders of magnitude (Taras et al. 2009). Thus, the residual strain is likely to play a much bigger role in estimates of the near-field ice loads. With the increase in the accumulated residual strains (Fig. 10), the departure of the normal stress from the thermal stress also showed a rough trend of increase).

Consequently, the real residual strain should be the sum of the present observed value and accumulated value prior to our investigation. Although the accumulation magnitude is not known, the real residual strain should certainly accounts for a much larger part of the thermal strain, namely, the real ice stress should be probably significantly lower than the present calculation.

Unfortunately the synchronous static stress of surface ice was not observed, so there were no direct evidences to support the present stress calculation. But a rough evaluation of the stress model performance can be done indirectly using field and tank observations at other sites (Yamaoka et al., 1988; Azarnejad and Hrudey, 1998; Morse et al., 2011; Petrich et al., 2015). The data pairs of diurnal increments in surface ice temperature $\Delta T_{diurnal}$ and the increment in ice stress $\Delta\sigma_{diurnal}$ were collected from the literatures and the present model results (Fig. 13). Generally, for a certain increase in ice temperature, the increase in ice stress was quite sparse due to varied

environmental conditions and physical and mechanical properties of ice. The present model was in a good agreement with the observations in a Hokkaido reservoir by Yamaoka et al (1988), but overestimated the ice stress at other sites. Several in situ measurements of thermal ice loads/stresses were conducted in northeastern China by Sui (1988). His findings at Shengli Reservoir, which is about 80 km northeast of Hongqipao Reservoir and is quite similar to the present reservoir with respect to hydrology, meteorology, and dam structure, showed that the near-surface ice stresses were 100~400 kPa, which is very close to the present calculations.

Although the physical parameters of freshwater ice were assigned with constant values (such as E and ν), these parameters are indeed temperature, strain rate and texture dependent (La Placa and Post 1960; Gold 1994; Han et al. 2015). Sensitivity tests of the model indicated that the ice stress/load is significantly sensitive to the variation in elastic modulus. Therefore, accurate parameterization of elastic modulus taking into account the effects of ice temperature and strain rate is expected to make the present model more competent.

Processes Affecting the Residual Strain

Static ice loads on hydraulic structures have been investigated extensively for decades. Thermal deformation of ice cover induced by the ice temperature changes is the predominant driver generating the ice strains/stresses and static loads. However, many processes modify the real ice strains/stresses and loads deviating significantly from the thermal ones. These processes include water level variations (Comfort et al 2003; Stander 2006; Taras et al 2009), wet crack development (e.g. parallel fractures and block upwarping) (Carter et al 1998; Comfort et al 2003; Taras et al 2009), ice-boundary bonding (Comfort and Liddiard 2006; Huang et al 2017), and dry surface crack development (Azamejad and Hrudey 1998). All of these processes introduce additional strains to the thermal strain. All additional strains are included in the residual strains herein, which were measured in large scales in this study.

The water level decreased monotonously through the whole ice covered period (Fig. 2) and dropped by approximately 5 cm over our measuring duration. If we assume the ice cover is equivalent to a thin disc with edge clamped to the dam and shore since its thickness is infinitely small compared to its horizontal size. According to the bending theory of thin disc with uniform

vertical loads, a 5 cm drop in water level causes an additional tensile stress of approximately 65 kPa (i.e. equivalent to a strain of 1.0×10^{-5}) to the surface of 1 m thick ice cover. This additional strain accounts for 14% of the total residual strain normal to the dam face. However, its real contribution is deemed to be much smaller than 14% because there were parallel fractures developed near and along the dam face (also in Huang et al (2013)). Parallel cracks have been frequently observed along dams and are generally located within 10 m from the dam for ice cover less than 1 m thick (Carter et al 1998; Stander 2006; Morse et al 2009). A continuous drop in water level largely makes the parallel cracks active and leads to new parallel cracks, hampering the ability of ice cover to bend.

Surface dry cracks were investigated using photography and image processing in this study . The crack density has a significant spatial variation. For instance, the crack density measured in a small area varies from 1% to 12%. These dry cracks usually are developed due to tension, compression, and shear history.

$$\$'' = \frac{\#\, l_i}{L_n}$$

$$\$'' = \frac{\$/}{\#}$$

Wind drag also creates ice stresses and loads on dam. Surface drag coefficient is assumed to be 1.5×10^{-3} (Prinsenberg and Petersen 2002), a strong wind with speed 10 m/s causes a shear stress of 0.2 Pa to the surface ice. For a fetch of 10 km (normal to the main dam line), the wind stress integrates to a line force of 2 kN/m on the dam face. These values are negligibly small compared the residual stress and calculated normal stress. However, the irregular shape of reservoir is expected to lead to a significant spatial variation in wind-induced line load on dam face especially around sharp corners.

Furthermore, some artificial activities (e.g. ice trench excavation in Ma and Li (2011)) and nearshore terrain (bathymetry) also influence the ice displacement, strain, and stress (Stander 2006). In order to better understand these processes and their impacts on ice loads, many more field efforts are still called for to gain experiences, especially on the impacts of the development and dynamics of dry and wet cracks, ice edge bonding situations, and creep behaviors of freshwater ice under .

Conclusion

With the help of a robust laser range finder, reservoir ice cover was monitored for displacements in the presence of incompletely confined boundaries, ice crack development, and water level drops, in response to thermal pressure. The recorded displacements of surface ice indicated that the real ice strain deviates significantly from the thermal strain. Residual strains were introduced and calculated from the displacement datasets. The residual strain is dependent when the measured range is less than about 12 m at this reservoir due to the spatial variation of crack development. It shows a similar diurnal and seasonal variation with air or ice temperature, but its daily amplitude is usually lower than the thermal strain. The water level fluctuations, parallel crack dynamics, surface (dry) cracks development and reservoir geometry have universal or site-specific impacts on residual strains.

The ice strain should consist of thermal strain and residual strain rather than the former alone used previously to estimate the ice stress. Both the ice strain and the residual strain are anisotropic largely due to the boundary shape. Although the principle strain and strain have similar trends with the thermal strain, the first principal is quite close to the thermal strain except during a sharp increase in ice temperature and . The normal strain is always lower than the thermal strain possibly due to strain release by the dynamics on the dam face, parallel fractures, upheavals of cracked ice blocks, dry crack development (Carter et al., 1998; Ma and Li, 2011).

A new constitutive model was account the residual strain. Using the observed residual strain, both principal and normal stresses (i.e. perpendicular to the dam) were estimated. The predicted normal stress is in an acceptable agreement with field measurements through indirect comparisons. The present model indicated that the residual strain/surface deformation has a significant impact on the surface ice stress.

, indicating that the residual strain is the key reason previous models. In this context one may wish to discriminate the impacts of ice boundary dynamics, crack development, and water level fluctuation on the residual st This is important and challenging so as to model the residual strain, and requires many more field

experiences and theoretical work.

Acknowledgments

This research was supported by the National Natural Science Foundation of China (No. 41402203 and 51579028) and the Special Fund for Basic Scientific Research of Central Colleges (310829171002). We are also grateful to Dr. Yu Yang from Shenyang Institute of Engineering, Mr. Yanfeng Cheng from Polar Research Institute of China, and the staff from the Executive Department of Hongqipao Reservoir for their field assistance and theoretical discussion.

References

Arunachalam, A.V.M. (2005). "Application of dimensional analysis to estimation of ice-induced pressures on rigid vertical structures." Can. J. Civil Eng., 32, 968–980.

Azarnejad, A., and Hrudey, T.M. (1998). "A numerical study of thermal ice loads on structures." Can. J. Civil Eng. 25, 557–568.

Bergdahl, L. (1978). "Thermal ice pressure in lake ice covers." Report Series A:2, Depart. Hydraul., Chalmers Univ. Technol., Goteborg, Sweden (164 pp).

Bouaanani, N., Paultre P., and Proulx J. (2004). "Dynamic response of a concrete dam impounding an ice-covered reservoir: Part I. Mathematical modelling." Can. J. Civil Eng. 31(6), 956–964.

Boulton, G.S., and Jones, A.S. (1979). "Stability of temperate ice caps and ice sheets resting on beds of deformable sediments." J. Glaciol., 24(90), 29–43.

Carter, D., Sodhi, D., Stander, E., Caron, O., and Quach, T. (1998). "Thrust in reservoirs." J. Cold Reg. Eng., 12(4), 169–183.

Comfort, G., Gong, Y., and Singh, S. (2000a). "Static ice loads for dam safety analysis." Proc. 3rd Can. Dam Safety Conf., Regina, Saskatchewan, Canada.

Comfort, G., Gong, Y., Singh, S., and Abdelnour, R. (2000b). "Predicting static ice loads on dams." Proc. 15th IAHR Int. Symp. on Ice, Gdansk, Poland, 135–143.

Comfort, G., Gong, Y., and Singh, S. (2000c). "The factors controlling static ice loads on dams." Proc. 15th IAHR

Int. Symp. on Ice, Gdansk, Poland, 189-197.

Comfort, G., Gong, Y., Singh, S., and Abdelnour, R. (2003). Static ice loads on dams. Can. J. Civil Eng., 30(1), 42-68.

Comfort, G., and Liddiard, A. (2006). Ice-induced damage to shoreline properties on Round and Golden Lakes. Proc. 18th IAHR Int. Symp. on Ice, Sapporo, Japan, 221-228.

Cox, G.F.N. (1984). A preliminary investigation of thermal ice pressures. Cold Reg. Sci. Techn., 9(3), 221-229.

Fransson, L. (1988). Thermal ice pressure on structures in ice covers. Ph.D. Thesis, Lulea Univ. Technol., Lulea, Sweden.

Fransson, L. (1991). Do cracks reduce thermal ice stresses? In Jones, S., Tillotson, J., Makenna, R. F., Jordaan, I. J. (eds) Ice-Structure Interaction, International Union of Theoretical and Applied Mechanics (International Association for Hydraulic Research). Springer, Berlin, Germany.

Gebre, S., Alfredsen, K., Lia, L., Stickler, M., and Tesaker, E. (2013). Review of ice effects on hydropower systems. J. Cold Reg. Eng., 27(4), 196-222.

Gold, L.W. (1994). The elastic modulus of columnar-grain freshwater ice. Ann. Glaciol., 19(2), 13-18.

Han, H., Jia, Q., Huang, W., and Li, Z. (2015). Flexural strength and effective modulus of large columnar-grained freshwater ice. J. Cold Reg. Eng., doi: 10.1061/(ASCE)CR.1943-5495.0000098.

Huang, W., Li, Z., Han, H., and Jia, Q. (2010). Limit resistive forces from ice frozen to concrete-revetment interface of an inclined dam wall. Cold Reg. Sci. Technol., 141, 1-8.

Huang, W., Lu, P., Lei, R., Xie, H., and Li, Z. (2016). Melt pond distribution and geometry in high Arctic sea ice derived from aerial investigations. Ann. Glaciol., 57(73), 105-118.

Ivchenko, A.B. (1990). Investigation of stress of ice cover under changes of temperature. Proc. IAHR 10th Symp. on Ice, Espoo, Finland, 149-157.

Jia, Q. (2012). Study on design ice parameters of slope protection on reservoir in cold regions. Doctoral Dissertation, Dalian University of Technology, Dalian, China. (in Chinese with English abstract)

Jia, Q., Li, Z., and Leppäranta, M. (2010). Estimation of annual maximum ice thickness in different return periods for a reservoir using air temperature. Proc. 20th IAHR Int. Symp. on Ice, Lahti, Finland.

Ko, P.K., Ho, M.S., and Smith, G..F. (1994). "Thermal ice forces on concrete dams recent developments." Proc. 1994 Can. Dam Safety Conf., Winnipeg, Manitoba, Canada, 1-37.

La Placa, S.J., and Post, B. (1960). "Thermal expansion of ice." Acta Cryst., 13(6), 503-505.

Ma, H., and Li, F. (2011). "A mechanism study on restricting static ice pressure by excavating trench method." Cold Reg. Sci. Technol., 66, 39-43.

Morse, B., Stander, E., Tatrai, A., Morse, J., Beaulieu, P., Taras, A., Nolin, P., and Pratt, Y. (2009). "Ice interactions at a dam face." Proc. 15th CRIPE Workshop on River Ice, CGU HS Committee on River Ice Processes and the Environment, St. John's, Newfoundland and Labrador

Morse, B., Stander, E., Richard, M., and Desmet, V. (2011). "Stress and strain dynamics in a hydroelectric reservoir ice sheet." Proc. 16th Workshop on River Ice, CGU HS Committee on River Ice Processes and the Environment, Winnipeg, Manitoba, Canada, 303-316.

Petrich, C., Sæther, I., Fransson, L., Sand, B., and Arntsen, B. (2006). "Time-dependent spatial distribution of thermal stresses in the ice cover of a small reservoir." Cold Reg. Sci. Technol., 120, 35-44.

Polashenski, C., Perovich, D., and Courville, Z. (2012). "The mechanisms of sea ice melt pond formation and evolution." J. Geophys. Res., 117, C01001, doi: 10.1029/2011JC007231.

Prinsenberg, S.J., Fowler, G.A., van der Baaren, A., and Beanlands, B. (1997). "Stress measurements from land-fast ice along Canada's Labrador Coast." Cold Reg. Sc. Technol., 25, 1-15.

Prinsenberg, S., and Peterson I.K. (2002). "Variations in air-ice drag coefficient due to ice surface roughness." Int. J. Offshore Polar Eng., 12(2), 121-1125.

Stander, E. (2006). "Ice stresses in reservoirs: effect of water level fluctuations." Cold Reg. Eng., 20(2), 52-67.

Sui, X. (1988). "Study on ice static pressure on ice cover reservoir." Proc. 9th IAHR Symp. on Ice, Sapporo, Japan, vol. 1, pp. 484-493.

Taras, A., Tatrai, A., Morse, B., Stander, E., Comfort, G., Nolin, P., Pratt, Y., and Lupien, R. (2009). "Measurement

of ice thrust on dams". Proc. CDA 2009 Ann. Conf., Whistler, British Columbia, Canada.

Timco, G. W., Watson, D. A., Comfort, G., and Abdelnour, R. (1996). "A comparison of methods for predicting thermally-induced ice loads". Proc. IAHR Ice Symp., Beijing China, 241-248.

Xu, B. (1986). "Design value of pressure due to expansion of ice sheet in reservoir". Proc. 8th IAHR Symp. on Ice, Iowa City, US, Vol. 1, 231-238.

Yamaoka, I., Fujita, M., and Hasegawa, K. (1988). "Measurement of thermal ice thrust exerted by an expanding ice cover in Taisetsu Dam Reservoir in Hokkaido, Japan". Proc. 9th IAHR Symp. on Ice, Sapporo, Japan, Vol. 1, 473-482.

Zhang, L., Li, Z., Jia Q., and Huang, W. (2012). "Experimental study on uniaxial compressive strength of reservoir ice". Trans. Tianjin Univ., 18(2), 112-116.

632 Table 1. Parameters and coefficients of freshwater reservoir ice for the stress model

Name	Symbol	Value
Elastic Modulus	E	1.5 GPa (Zhang et al. 2012; Han et al. 2015)
Expansion coefficient	%	5.0' 10^{-5}/¡C
Viscous creep rate	K	KD = ! #($\frac{T_*}{T}$)^m, where& =2.46' 10^{29}/s, T$_*$ =-1¡C, m =1.92 (
Coefficient of viscous deformation	D	Petrich et al. 2015)
Coefficient	n	3.7 (Petrich et al. 2015)
Reference stress	S_0	100 kPa
Time step	h	1800 s
Initial stress	$S_{(0)}$	10 kPa

633
634

635

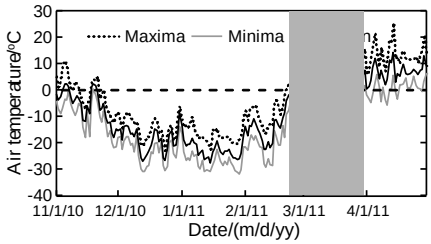

636

637 Fig. 1. Daily air temperature during winter 2010–11 from Anda meteorological station. The time

638 series is in good agreement with our field data (Jia et al. 2010). The field experiment period is

639 highlighted grey.

640

641

642

643 Fig. 2. Water level variation in Hongqipao reservoir during the ice season 2010–2011 (Day 305

644 denotes Nov. 1, 2010).

645

646

647 Fig. 3. The location of Hongqipao reservoir and the layout of instrumentation site (Google Earth).

648

649

650 Fig. 4. Ice cover displacement within different confined boundaries. Points O and Pi denote the

651 positions of LRF and reflector, respectively. L_L, L_T, and L_B denote the distances between O and Pi

652 after a temperature increase for fixed (a), free (b), and (c) ends,

653 respectively.

654

655

656

657

658 Fig. 5. The ice edge dynamics on the dam face and the development of cracks.

659

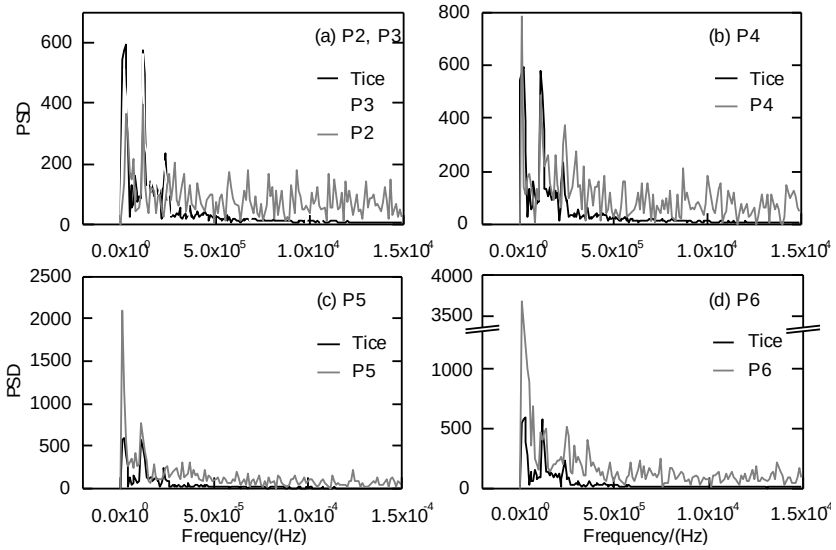

660

661 Fig. 6. Power spectrums for directional displacements and ice temperature. PSD is short for power

662 spectral density.

663

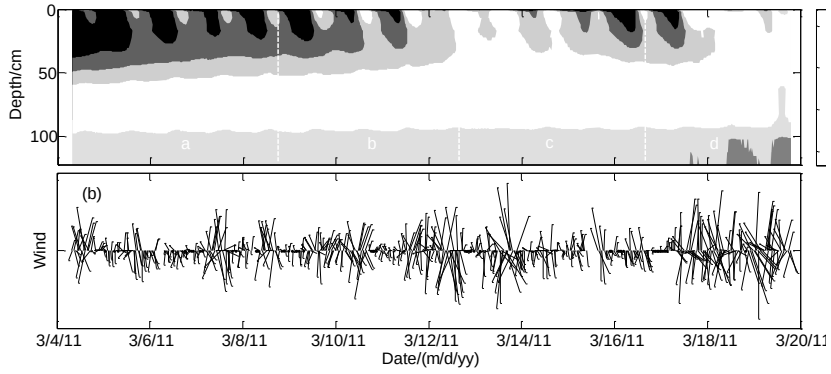

664

665 Fig. 7. Ice temperature (a) and wind series (b) during the campaign, divided into four phases (a–d).

666 The depth was below ice surface (0 cm). Data at 102 and 122 cm depths show actually

667 temperatures of water under ice.

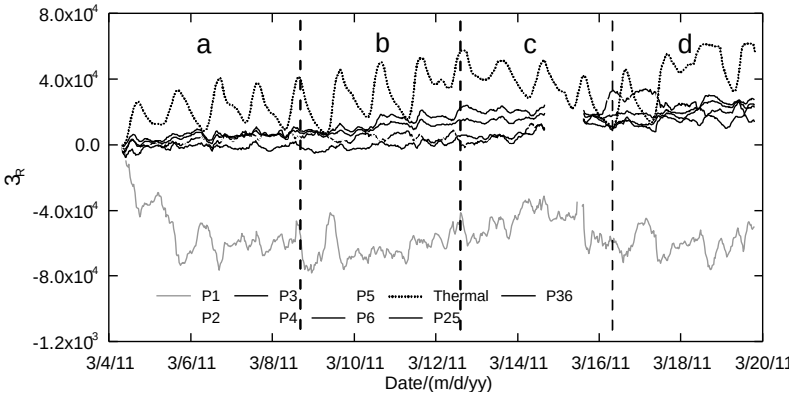

668

669 Fig. 8. The observed and thermal strain from March 4 to 20 in 2011.

670

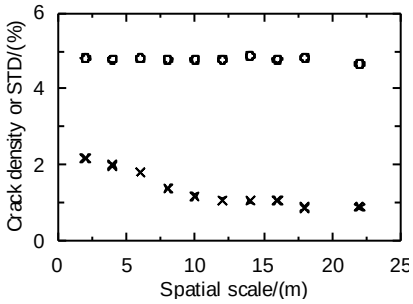

671

672 Fig. 9. The crack density! () and its standard deviation (STD), at different spatial scale over the

673 ice cover surface.

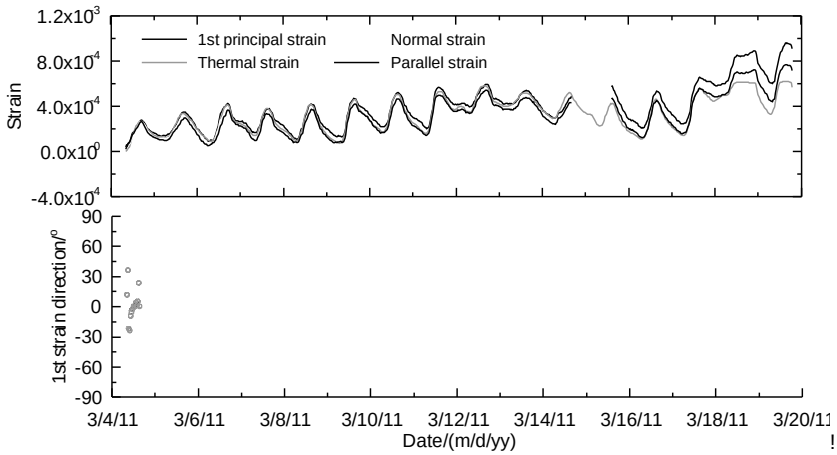

674 !

675 Fig. 10. The first principal strainb() and its directionc()

676 . The direction of the first principal strain is

677 positive counterclockwise with the zero pointing to the north. The normal parallelstrain